

Numerical study of internal flue gas recirculation system applied to methane-hydrogen powered gas microturbine combustor

ARTICLE INFO

Received: 9 May 2022
Revised: 11 July 2022
Accepted: 20 July 2022
Available online: 24 July 2022

Sources of renewable energy have been increasingly used all over the world. This kind of energy is highly desirable because of its unlimited availability. Unfortunately, renewable energy production very much depends on weather conditions. Consequently, it is necessary to store the produced excess energy in order to use it when needed. There is a technology able to produce a hydrogen/methane fuel from excess renewable energy, which may be stored. This technology is called the Power-to-Gas technology (P2G). Since the efficiency of this technological process depends on the hydrogen fraction in the renewable energy fuel, there is a need to increase this fraction. Concurrently, the gas microturbine technology is increasingly widely used in various industries (aviation, energy, automotive, military, etc). The P2G technology and the gas microturbine technology are likely to be integrated in the near future and, as mentioned above, the hydrogen fraction in the methane-hydrogen fuel will tend to increase. In order to power a gas microturbine with the methane-hydrogen fuel, it will be necessary to modify the combustor to avoid an excessive temperature increase and flashbacks. In this paper it is proposed to apply an autonomous internal exhaust gas recirculation system to resolve the hydrogen combustion problems indicated above. The operating principle and the proposed design of the recirculation system and the latter's impact on the combustor's operating parameters and emissivity (NO_x and CO) are presented.

Key words: gas microturbines, combustor, power-to-gas, hydrogen, exhaust gas recirculation

This is an open access article under the CC BY license (<http://creativecommons.org/licenses/by/4.0/>)

1. Introduction

1.1. Integration of power-to-gas technology and gas microturbine technology

An increase in electricity supply from renewable energy sources, especially from wind turbines, hydroelectric power plants and photovoltaic panels, can be observed in the power generation sector. Renewable energy sources present many advantages, such as unlimited energy production. One of the major drawbacks of all the energy sources is that the energy production is not constant over time, being variable and intermittent mainly due to weather conditions. This problem can be addressed by storing the excess energy and using it when convenient. It is possible to transform (through hydrolysis) the excess electrical energy into hydrogen and then to produce methane (using carbon dioxide, previously generated hydrogen and electrical power in a process called methanation). Finally, the two gases, i.e. hydrogen and methane, are mixed to obtain a renewable fuel. This technology is called “power-to-gas” (“P2G”) [1]. The presence of methane gas in the renewable fuel makes the production of the latter less efficient than if solely hydrogen was used, but it is necessary because of the specific properties of hydrogen – hydrogen is more difficult and dangerous to store and transport and more demanding as regards its use in power devices [2]. In order to optimise the use of this renewable source energy, the percentage of hydrogen in the renewable fuel produced using the P2G technology needs to be increased.

Today, gas microturbines are increasingly often used in various industry sectors: in aviation to power drones, in the automotive industry to extend a car's range (e.g. Jaguar CX75, Pininfarina H600, etc.), in the energy industry to generate electrical (and heat) power for house applications,

and so on [3]. Gas microturbines present many advantages, such as low noise level, cheap operation, limited number of moving parts, low emissions, etc. [4]. Consequently, the use of gas microturbine technology has spread to many industry sectors.

It can be beneficial to integrate the P2G technology and gas microturbine devices. For this purpose the efficiency of P2G should be increased by using a more hydrogen enriched fuel and the combustors of the latter need to be adapted. The use of a more hydrogen enriched fuel provokes higher local combustion temperatures and higher flame velocities [5], whereby if the combustors were unmodified, this would result in local overheating and increased NO_x emissions and provoke flame flashbacks in the direction of the fuel injection zone. All of this would have an adverse effect on the operation of the microturbine devices.

1.2. Exhaust gas recirculation applied to gas micro-turbines

In order to avoid the problems connected with the use of a more hydrogen enriched fuel in gas microturbines, conventional (diffusion) gas microturbine combustors must be made capable of reducing the combustion temperature and moving the combustion zone towards the exhaust outlet (to avoid flame flashbacks). In order to propose a solution to the above problems, a review of the literature on the subject was carried out and is presented below.

Guethe et al. [6] investigated the impact of exhaust gas recirculation (from the turbine outlet to the compressor inlet) in gas turbines. Turning back exhaust gases entails a reduction in the amount of oxygen in the combustion zone and an increase in carbon dioxide concentration. From the point of view of the chemical combustion process the re-

duction in the amount of combustion zone oxygen limits the concentration of O radicals which drive the combustion process. It is noted that carbon dioxide is not a gas “perfectly inert” in the combustion process. This means that some of the carbon dioxide present in the combustion process is subject to a certain reaction. The latter was identified as: $\text{OH} + \text{CO} \leftrightarrow \text{H} + \text{CO}_2$. Thus carbon dioxide can react with hydrogen atom H which is one of the radicals in the combustion process. Thanks to this reaction one can reduce the amount of hydrogen radicals in the combustion process and at the same time increase the OH and CO species. The research carried out by Liu et al. [7] drew attention to the fact that hydrogen radical H is involved in the combustion process in the following reaction: $\text{H} + \text{O}_2 \leftrightarrow \text{O} + \text{OH}$. Given that carbon dioxide reduces the amount of the hydrogen radicals present, the above-mentioned reaction is also reduced. This, in turn, limits the generation of O and OH substances (which are also radicals), whereby the combustion process reaction is significantly affected. According to Guethe et al. [6] and Liu et al. [7], limiting the concentration of hydrogen and oxygen radicals in the combustion zone carbon dioxide has a strong impact on the combustion process by inhibiting the combustion reaction, which results in a reduction in the combustion temperature and in a decrease in the laminar flame speed.

Ditaranto et al. in [8] showed that owing to the higher specific heat capacity of steam the use of steam dilution to limit the combustion temperature in gas turbine combustors is more effective than the use of nitrogen dilution. Hence by introducing a species whose specific heat capacity is higher than that of air one can reduce the combustion temperature in a gas turbine combustor. The recirculated turbine exhaust gases contain pure exhaust gases. The latter consist mainly of carbon dioxide and steam. Above 550 K the specific heat capacity of carbon dioxide and steam at a constant pressure is higher than that of air at the constant pressure [9–11]. Near the liner of the gas microturbine combustion chamber the temperature ranges from 770 K to as high as 2300 K [12]. The evolution of the specific heat capacity of the above-mentioned species at the constant pressure of 1 bar is presented in Fig. 1.

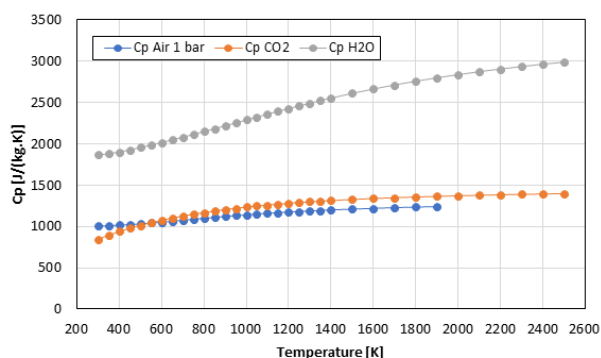


Fig. 1. Heat capacity of air, carbon dioxide and steam at constant pressure of 1 bar

In the combustion chamber operating conditions the specific heat capacity of the exhaust gases at a constant pressure is higher than that of the air supplied to the com-

busion chamber. Therefore the exhaust gases recirculated into the combustion zone will be able to absorb more combustion heat, whereby the temperature in the combustion zone will decrease. Hence it can be concluded that thanks to the physical action of the exhaust gases it will be possible to reduce the combustion temperature peak and gradient. As a result, the rate of combustion of the laminar flame will also be reduced (according to van't Hoff's law, as the temperature of a chemical reaction decreases, the reaction rate also decreases). Preliminary analyses indicate that the reintroduction of some of the exhaust gas into the combustion zone would provoke a reduction in both combustion temperature and flame speed.

Shi et al. [13] carried out research on a burner equipped with an Internal Flue Gas Recirculation (IFGR) system and demonstrated that by reintroducing some of the exhaust gas into the burner's air inlet one can increase the combustion zone volume, causing a reduction in combustion temperature, whereby the emission of nitrogen oxides can be reduced. The temperature reduction strongly depends on the combustion volume increased.

It emerges from the above that the introduction of an exhaust gas recirculation system into the gas microturbine combustor is an interesting solution. The presence of exhaust gases acts physically and chemically on the combustion process, limiting its combustion temperature, peak combustion temperature and combustion velocity. The recirculation of exhaust gases into the gas microturbine combustor would potentially reduce the combustion temperature and velocity, whereby hydrogen could be added to the fuel while keeping the nominal operating parameters and emissivity. Moreover, by adding more hydrogen to the fuel a reduction in the emission of carbon species, such as hydrocarbons and carbon monoxide, would be achieved. For the purpose of internal exhaust gas recirculation it is proposed to create a pipe system integrated into the combustor, able to autonomously move the exhaust gases from the exhaust outlet into the combustion zone. This concept is detailed in part II of this paper.

Other studies show that the application of exhaust gas recirculation may have a negative effect on the combustion process. These studies are presented below.

The fact that the exhaust gases contain some carbon monoxide needs to be taken into consideration. Jadidi et al. [14] and Taamallah et al. [15] presented the adiabatic temperatures of selected combustibles. The adiabatic combustion temperature of carbon monoxide is very high in comparison with that of hydrogen and can reach 2450 K. This temperature is higher than the adiabatic combustion temperature of methane fuel (2250 K) or hydrogen fuel (2400 K). This is why as a result of the recirculation of exhaust gases containing carbon monoxide the combustion temperature can increase in comparison with the case without recirculation.

One should also note that the recirculation of exhaust gases provokes a replacement of some of the “fresh” air coming from the compressor by a portion of the “hot” exhaust gases in the primary combustion zone. This results in an increase in the enthalpy of the gases supplied into the

combustion zone, increasing the peak temperature and the temperature gradients in the primary combustion zone.

Gieras [12] presented a concept of adapting the liner's holes to optimise the combustion process in a jet micro-turbine. In this way the mass flow passing through the combustor is effectively modified in various operating conditions. The introduction of an IFGR system into the combustor can modify the combustion process by creating or extending a combustion zone with an air-fuel equivalence ratio close to unity. This phenomenon can be responsible for an increase in combustion temperature.

The above three arguments show that the introduction of some of the exhaust gas into the combustion zone can have an opposite effect to the intended one. The replacement of some of the fresh air coming from the compressor by a part of the hot exhaust gases in the primary combustion zone and the potential modification of the air-fuel equivalence ratio may be responsible for an increase in combustion temperature.

It emerges from the above literature review that the introduction of an autonomous recirculation system (IFGR) into the gas microturbine combustor can have a positive or negative effect on the combustion process, particularly in the case of hydrogen enriched fuel. In order to determine the effect of the IFGR system on the combustion process (with and without hydrogen addition), the research presented below was carried out.

1.3. Novelty of this research

In the last decade of the 20th century a new approach to combustion, dedicated to industrial furnaces, was developed. This combustion method, referred to as High Temperature Air Combustion (HiTAC) [16], was developed by the Japanese company Nippon Furnace Kogyo (NFK) [17]. Other similar combustion technologies, diversely referred to as: Flameless Combustion (FLC), Flameless Oxidation (FLOX) and Moderate and Intense Low-oxygen Dilution (MILD) [18], were subsequently developed. All these methods are based on injecting hot air and fuel at high velocity into the combustion chamber. The air-fuel mixture temperature is higher than the auto-ignition temperature of the fuel. A recirculation zone is generated whereby the combustion products are diluted with the exhaust gases. As a result, the combustion zone spreads throughout the chamber volume. The temperature field is much more homogeneous than in the case of conventional combustion. Thanks to the homogeneous combustion zone the emissivity of NO_x and CO species is reduced [19]. All these combustion technologies are often grouped under the designation "MILD combustion" [18]. The MILD combustion process can be widely applied to various energy devices [20]. Recently this technology was studied to be applied to gas turbines [16] and even to gas microturbines [21]. The major challenge of conducting MILD combustion in a gas (micro)turbine is to keep the combustor inlet temperature above the auto-ignition temperature of the fuel [22]. This challenge inhibits the application of MILD combustion to gas microturbines. Considering this difficulty, an alternative concept to the MILD combustion design, suitable for the conventional gas microturbine combustor burning a more hydrogen enriched methane fuel is proposed in this paper.

The power-to-gas technology and the gas microturbine technology are very useful and widely used. In order to better integrate the two technologies, an effort must be made in the near future to increase the hydrogen fraction in the fuel mixture used in the gas microturbine. According to the presented literature review, this goal can be achieved by incorporating an autonomous internal flue gas recirculation system into the gas microturbine combustor. The aim of the present research was to assess through numerical analyses the usefulness of applying IFGR to a gas microturbine for the purpose of burning a more hydrogen enriched fuel. A conventional diffusion combustor was designed and then its design was modified by adding a pipe system enabling the autonomous exhaust gas recirculation inside the combustor. The following were assessed:

- the possibility of effecting autonomous IFGR inside the gas microturbine combustor
- the modification of the combustor's main operating parameters (the total pressure drop and the total exhaust gas temperature) by the IFGR system
- the impact of the IFGR system on the temperature field in the combustion zone
- the impact of the IFGR system on the CO and NO_x concentrations in exhaust.

Each of the evaluations was carried out for the hydrogen mass fraction in the methane fuel ranging from 0 to 0.5. The study was conducted using the numerical tools described further in this paper.

The novelty of this research consists in numerically investigating a novel IFGR system applied to the gas micro-turbine to evaluate its positive or negative impact on the combustor operation.

2. Case study combustor and operating conditions

A reference combustor was designed for a 40 kW gas microturbine powered by methane fuel. The combustor's approximate operating parameters are presented in Table 1. The combustor is schematically shown and described in Fig. 2.

Table 1. Reference gas microturbine and combustor operating parameters

| Parameters | Combustor inlet | Combustor outlet |
|--|-----------------|------------------|
| p* [Pa] | 324992.333 | 311992.640 |
| p [Pa] | 306584.082 | 301133.803 |
| T* [K] | 433.834 | 1185 |
| T [K] | 426.666 | 1175.062 |
| c [m/s] | 120 | 155 |
| $c_s = 4.874 \cdot 10^{-3} \frac{\text{kg}}{\text{s}}; \dot{m} = 0.251 \frac{\text{kg}}{\text{s}}$ | | |

The first main objective of this study was to assess the possibility of effecting autonomous internal exhaust gas recirculation by adding a pipe system. The challenge consisted in moving exhaust gases from the combustor outlet zone to the top part of the liner. The pressure drop occurring in the combustor made this task difficult. Many IFGR pipe systems were analysed to find the ones most suitable for this application. Two IFGR systems (presented below) were selected.

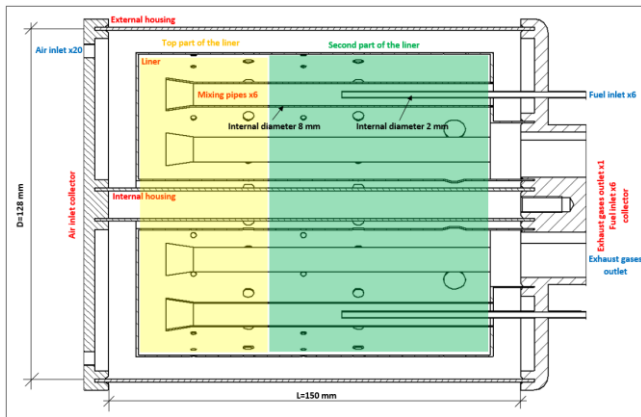


Fig. 2. Cross sectional view of 3D model of reference combustor

Figure 3 shows the first modified combustor equipped with an IFGR system (case A). In this case, a pipe system is installed between the liner and the combustor’s external housing, whereby some of the exhaust gas can be transferred from the combustor outlet zone to the top part of the liner. The difference between the total pressure at the combustor outlet and the static pressure at the top of the liner is used to enable exhaust gas recirculation. Figure 4 shows the second modified combustor equipped with the IFGR system (case B). In this case, the mixing pipes are modified in two

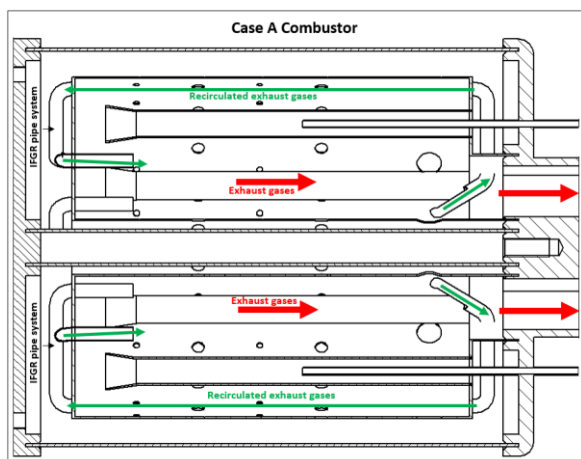


Fig. 3. Cross sectional view of 3D model of modified combustor (case A)

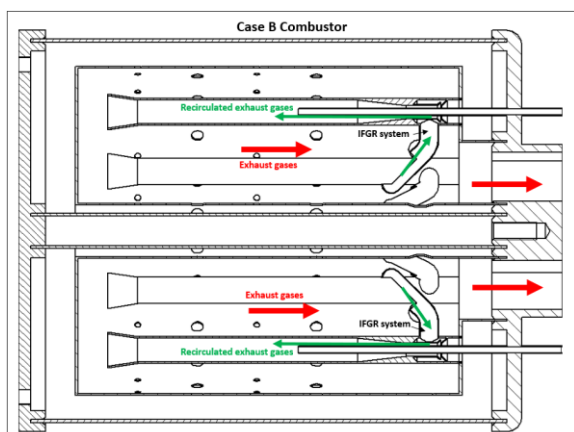


Fig. 4. Cross sectional view of 3D model of modified combustor (case B)

ways. Firstly, pipes taking some of the exhaust gas from the combustor outlet and introducing it into mixing pipe air are added to the mixing pipes. This design exploits the difference between the total pressure at the combustor outlet and the static pressure inside the mixing pipe. Secondly, the interior of the mixing pipes is shaped into a venturi, which increases the pressure difference and improves exhaust gas recirculation.

3. Numerical methods

3.1. Computational domain mesh system

3D combustor models were created using Solid Edge and the Ansys pre-processor [23]. Mesh generation is a major step in the simulation of the combustor. As it yields accurate results, the tetrahedral mesh structure is often used for gas microturbine combustor simulations [24–28]. The tetrahedral mesh can be applied to a complex geometry while maintaining acceptable values of quality parameters (skewness, orthogonality and aspect ratio). Recently, the polyhedral cell mesh has been intensively developed. Similarly as the tetrahedral mesh, polyhedral cells give relatively accurate results at better quality parameters [29–31]. A polyhedral mesh with the maximum cell length of 0.8 mm was selected for this study. After mesh volume generation the obtained mesh was improved by selecting the value of 0.45 as the desired minimum orthogonal quality. Finally, boundary layers were generated in order not to exceed the Y^+ value of 300. According to the literature [24–25], the obtained grids (and the numbers of elements) constituting the calculation domains are sufficient to provide reliable results. The computational domain is shown in Fig. 5. Table 2 shows the quality parameters of the mesh.

Table 2. Mesh quality parameters

| Case | Number of cells [millions] | Maximum aspect ratio | Maximum skewness | Minimum orthogonal quality |
|-----------|----------------------------|----------------------|------------------|----------------------------|
| Reference | 5.8 | 38.3 | 0.895 | 0.435 |
| Case A | 7.0 | 35.8 | 0.900 | 0.432 |
| Case B | 6.4 | 62.0 | 0.895 | 0.200 |

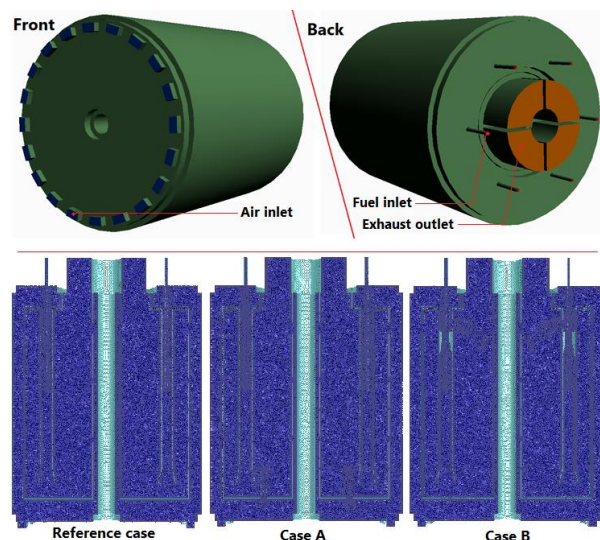


Fig. 5. External view of computational domain (external view is similar in all cases) and the mesh view in longitudinal cross sections for each combustor cases

3.2. Mathematical model

The simulations performed in this study were based on the CFD Ansys code [32]. The following processes: the turbulent flow, the non-premixed combustion in the gas phase and the radiative heat exchange, taking place within the calculation domain, were modelled as part of this study of the gas microturbine combustor.

The realizable $k-\epsilon$ model [12, 33] was used to model the turbulent flow through the combustor. This model is a Reynolds Averaged Stokes-Navier model (RANS). The realizable $k-\epsilon$ turbulence model is widely used to model flows in many industrial applications. This model yields acceptable results at a low computational cost. The enhanced wall treatment was enabled. The enhanced wall treatment makes it possible to fully resolve the flow on the wall boundary when Y^+ is less or equal to 1, or to apply the enhanced wall function when Y^+ is greater than unity. The enabled wall treatment model is a good compromise when wall phenomena are not of crucial importance for the studied flow properties, as it is the case in this study.

In the studied combustor cases the radiation model had to be enabled to model the heat exchanges inside the calculation domain, next to the heat transfer via conduction and convection. Radiation needs to be modelled in order to perform an accurate simulation and it is one of the most complex phenomena to be modelled. The Discrete Ordinate model [12, 25], which considers the calculation domain as a grey body, was used to model the radiation phenomena. The two major radiation absorbers and emitters in the combustor are steam and carbon dioxide. To perform a correct radiation simulation, it is necessary to use the Weighted Sum of Grey Gases method [12]. Emissivity coefficients extracted from the benchmark exponential wide-band model [34] were used in the simulation. The total gas phase absorption coefficient was calculated from the total emissivity with the mean path length calculated from the characteristic cell size. Wall emissivity was set to unity, which is a typical recommendation in gas microturbine combustor simulations [35].

The non-premixed steady diffusion flamelet [36] model was used to model turbulent combustion. In this model the flames in a turbulent flow are considered as a set of steady laminar flames referred to as “flamelets”. Using this model one can apply a detailed chemistry model taking into account the kinetics effects. This combustion model also takes local turbulence phenomena into account through strain rates. A look-up table is generated before the calculations are run. Using the look-up table one can present the flame’s all physical and chemical properties as a function of the mixture fraction in each location in the calculation domain. The local mixture fractions are determined on the basis of the flow turbulence. Hence the model enables one to determine the flame properties as a function of the mixture fraction and the local turbulence. The model yields sufficiently accurate results at a moderate computing cost.

The flamelets used in the non-premixed combustion model were generated on the basis of the detailed GRI-MECH 3.0 chemistry mechanism [37]. This mechanism takes into account 53 species involved in 325 reactions. From the GRI-MECH 3.0 website [37] the mechanism data and thermodynamic data files were freely downloaded and

then inserted into the Ansys Fluent software using the non-premixed combustion model dialogue window. Before generating the flamelets, the hydrogen (H_2) and methane (CH_4) mass fractions in the fuel had been selected. In this study the hydrogen mass fraction evolved from 0 to 0.5 at a step of 0.1. For this range of the hydrogen mass fraction in the fuel the selected GRIMECH 3.0 mechanism gives sufficiently accurate results [38]. The oxidizer (air) composition was simplified to the 0.23 mass fraction of oxygen (O_2) and the 0.77 mass fraction of nitrogen (N_2). For each fuelling case individual set of flamelets was created. Based on the individual flamelet sets, the individual probability density function (PDF) tables were generated.

Finally, boundary conditions were determined. The inlet is the “mass flow” and the outlet is the “pressure outlet” (the values of the respective quantities were taken from the combustor design calculations). The x-velocity at the outlet was initially assumed to be the same as the velocities immediately upstream of the outlet plane and scaled appropriately to respond to the overall mass conservation. At the outlet plane $(\partial\phi/\partial x)_{exit} = 0$. At the calculation domain’s wall the no slip condition was enabled and the velocity values were set to zero. Near to the wall the flow is more affected by molecular viscosity than by turbulence phenomena. The wall function method presented in [39], which uses algebraic formulations to link the quantities at the wall to those occurring further away, was applied. The boundary conditions are described in Table 3.

Table 3. Boundary conditions obtained from simulations

| Boundary condition designation | Type | Parameters |
|--------------------------------|-----------------|---|
| Air inlet | Mass-Flow Inlet | Mass flow = 0.251 kg/s Turbulent Intensity = 15% Turbulent Viscosity Ratio = 10 Total Temperature = 433.834 K Mean Mixture Fraction = 0 Mixture Fraction Variance = 0 |
| Fuel inlet | Mass-Flow Inlet | Mass flow = variable (see Table 4) Turbulent Intensity = 15% Turbulent Viscosity Ratio = 10 Total Temperature = 300 K Mean Mixture Fraction = 1 Mixture Fraction Variance = 0 |
| Exhaust | Pressure Outlet | Static Pressure = 0 Pa Turbulent Intensity = 15% Turbulent Viscosity Ratio = 10 Backflow Total Temperature = 300 K Mean Mixture Fraction = 0 Mixture Fraction Variance = 0 |
| Wall | Wall | Stationary Wall No Slip No Heat Exchange Internal Emissivity = 1 Opaque Wall Diffuse Fraction of Radiation = 1 |
| Operating conditions | – | Operating pressure = 301133.803 Pa Gravity off |

The second-order discretization [25] with the pressure-velocity coupled method and the pseudo-transient option enabled [40] was applied. The pressure-based solver [25, 40] was used for these series of simulations. Once the setup was completed the simulations were run.

In order to determine the fuel mass flow to be supplied into the combustor as a function of the hydrogen mass fraction in the fuel it was assumed that the total energy supplied into the combustor in the reference case (methane powered) had to be maintained. The lower heating values (LHV) of methane and hydrogen ($LHV_{CH_4} = 50$ MJ/kg and $LHV_{H_2} = 120$ MJ/kg [1]) were used in formula 1. The calculation results are presented in Table 4.

$$C_s^{iH_2mass_fraction} = \frac{LHV_{CH_4} \cdot C_s^{oH_2mass_fraction}}{LHV_{H_2} \cdot H_2mass_fraction + LHV_{CH_4} \cdot (1 - H_2mass_fraction)} \quad (1)$$

Table 4. Fuel mass flows as function of hydrogen mass percentage in fuel

| H ₂ mass percentage [%] | $C_s^{iH_2mass_fraction}$ [kg/s] |
|------------------------------------|-----------------------------------|
| 10 | 0.004252 |
| 20 | 0.003787 |
| 30 | 0.003413 |
| 40 | 0.003107 |
| 50 | 0.002851 |

4. Results and discussion

As part of this study, the ability to effect autonomous exhaust recirculation was analysed for various hydrogen mass fractions in the methane fuel. The impact of the IFGR system implementation on the pressure drop and on the combustion processes was assessed by analysing the temperature fields, the air-fuel equivalence ratio and the evolution of CO and NO_x concentrations in exhaust.

4.1. Exhaust gas recirculation rate

The numerical simulation results for the three cases are discussed in this subsection. Numerical simulations showed that it was possible to obtain autonomous exhaust gas recirculation inside the gas microturbine combustion chamber at the maximum global rate of 0.53%. The IFGR system was found to affect the combustion processes without significantly modifying the combustor operating parameters. The pipe air, fuel and exhaust gas flows through the combustor's mixing pipes for different cases and different hydrogen mass fractions in the methane fuel are presented in Table 5. Figure 6 shows the recirculated exhaust gas mass flows for cases A and B and different hydrogen mass fractions in the methane fuel.

Table 5. Mass flows after IFGR system implementation

| Case | Mass flow leaving all pipes [kg/s] | Exhaust mass flow recirculated by IFGR [kg/s] | Fuel mass flow entering in all pipes [kg/s] | Air mass flow entering in all pipes [kg/s] |
|-------|------------------------------------|---|---|--|
| R00H2 | 3.706E-02 | 0 | 4.874E-03 | 3.219E-02 |
| R10H2 | 3.582E-02 | 0 | 4.252E-03 | 3.156E-02 |
| R20H2 | 3.502E-02 | 0 | 3.787E-03 | 3.124E-02 |
| R30H2 | 3.449E-02 | 0 | 3.413E-03 | 3.108E-02 |
| R40H2 | 3.425E-02 | 0 | 3.107E-03 | 3.114E-02 |
| R50H2 | 3.433E-02 | 0 | 2.851E-03 | 3.148E-02 |
| A00H2 | 3.751E-02 | 8.236E-04 | 4.874E-03 | 3.263E-02 |
| A10H2 | 3.613E-02 | 8.749E-04 | 4.252E-03 | 3.188E-02 |
| A20H2 | 3.541E-02 | 8.703E-04 | 3.787E-03 | 3.163E-02 |
| A30H2 | 3.490E-02 | 8.577E-04 | 3.413E-03 | 3.149E-02 |
| A40H2 | 3.460E-02 | 8.588E-04 | 3.107E-03 | 3.149E-02 |
| A50H2 | 3.463E-02 | 8.373E-04 | 2.851E-03 | 3.178E-02 |
| B00H2 | 2.538E-02 | 1.344E-03 | 4.874E-03 | 1.916E-02 |
| B10H2 | 2.476E-02 | 1.269E-03 | 4.252E-03 | 1.924E-02 |
| B20H2 | 2.417E-02 | 1.208E-03 | 3.787E-03 | 1.917E-02 |
| B30H2 | 2.383E-02 | 1.188E-03 | 3.413E-03 | 1.923E-02 |
| B40H2 | 2.347E-02 | 1.154E-03 | 3.107E-03 | 1.920E-02 |
| B50H2 | 2.316E-02 | 1.126E-03 | 2.851E-03 | 1.919E-02 |

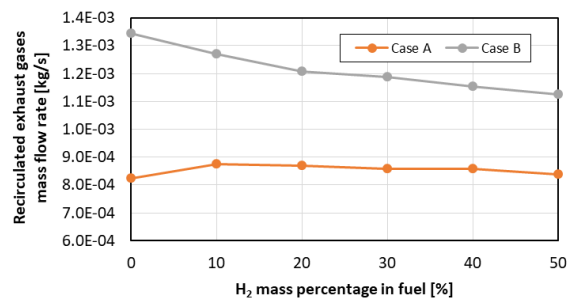


Fig. 6. Recirculated exhaust gas mass flows

The simulations yielded the recirculated exhaust gas mass flows for each of the combustor cases. IFGR ratios were calculated from equations 2 and 3. IFGR% stands for the ratio of the recirculated exhaust gas mass flow to the air mass flow passing through the mixing pipe, while IFGR%* stands for the ratio of the recirculated exhaust gas mass flow to the exhaust gas mass flow leaving the combustor. Figure 7 shows the calculated IFGR ratios.

$$IFGR\% = \frac{\text{Recirculated exhaust gas mass flow}}{\text{Air mass flow passing through mixing pipe}} \cdot 100 \quad (2)$$

$$IFGR\%^* = \frac{\text{Recirculated exhaust gas mass flow}}{\text{Exhaust gas mass flow leaving combustor}} \cdot 100 \quad (3)$$

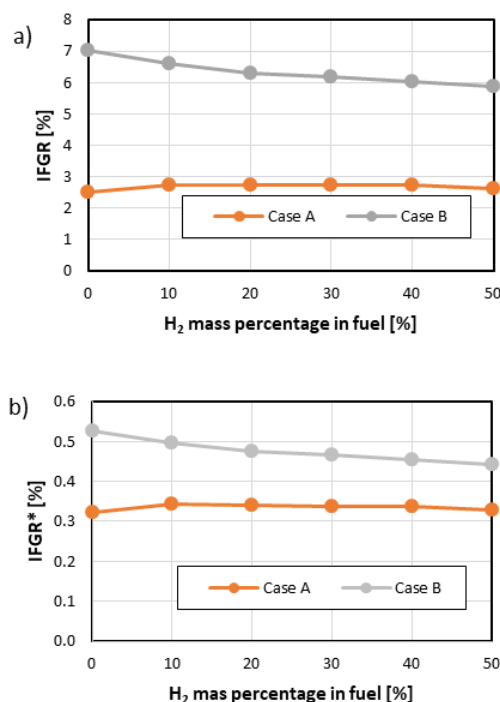


Fig. 7. a) IFGR ratio and b) IFGR* ratio

Firstly, it appears from the above that the IFGR% and IFGR%* ratios in case B are higher than in case A, regardless of the hydrogen mass fraction in the methane fuel. Figure 7 shows that in case A the IFGR% ratio ranges from 2.52 to 2.75%, whereas in case B it ranges from 5.87 to 7.01%. In case A the IFGR%* ratio is in the range of 0.32–0.34%, versus 0.44–0.53% in case B. The difference be-

tween these cases is due to design differences. In case A the recirculation of exhaust gases is accomplished by creating a pressure difference between the collection and injection locations. The difference between the total pressure (in the location where the exhaust gases are collected) and the static pressure (in the location where the exhaust gases are released) is exploited. In case B the recirculation of exhaust gases is driven not only by the total-static pressure difference, but also by an additional pressure difference generated by the venturi shaped mixing pipe. Due to this difference in the IFGR system design the amount of recirculated exhaust gases is greater in case B than in case A.

Secondly, one should note that in case A the IFGR ratios are constant, whereas in case B the IFGR ratios decrease as the hydrogen mass fraction in the fuel increases. In both cases this observation is fully concordant with the IFGR system design. In case A exhaust gases are recirculated by a pipe system located between the liner and the combustor's external housing, while in case B the IFGR system is directly connected to the mixing pipe inside the liner. The modification of the fuel's composition by adding hydrogen to the methane results in the diminution in the density of the fuel in the fuelling pipes and provokes an increase in the velocity of the fuel leaving the fuelling pipes. Once the fuel enters the mixing pipe, its velocity decreases, while its static pressure increases. In case B this results in a reduction in the pressure difference in the venturi fuelling pipe section, whereby the recirculated exhaust gas mass flow decreases as the hydrogen mass fraction in the fuel increases. In case A the IFGR system is independent of the phenomena arising inside the mixing pipes, whereby the IFGR ratios are constant regardless of the hydrogen mass fraction in the fuel.

Finally, let us consider the risk of IFGR system overheating depending on the IFGR system design. In case A, the IFGR system is a set of pipes located between the liner and the combustor's external housing. This design reduces the risk of IFGR system overheating since the set of IFGR pipes is constantly cooled by the air exiting the compressor. In case B, the IFGR system is located in the combustor outlet zone, far from the main combustion temperature, whereby the risk of IFGR system overheating is reduced. In both cases the IFGR system design reduces the risk of IFGR system overheating.

Summing up, it is possible to achieve autonomous exhaust gas recirculation inside a gas microturbine combustor for various hydrogen mass fractions in the fuel if an adequate IFGR pipe system is used. The IFGR ratios are constant in case A, while in case B the ratios decrease as the hydrogen mass fraction in the fuel increases. The case B IFGR system enables quantitatively larger exhaust gas recirculation than case A, regardless of the hydrogen mass fraction. In case A the IFGR%* ratio is about 0.33%, while in case B this ratio amounts to about 0.50%. In both cases the IFGR system design reduces the risk of IFGR system overheating.

4.2. Impact of IFGR system on pressure drop

In this subsection the total pressure drop in the combustion chamber is analysed. Figure 8 shows the total pressure drop for each combustor case and for various hydrogen

mass fractions in the fuel. The total pressure drop is calculated from equation 4.

$$\Delta p^* = \frac{p_2^* - p_3^*}{p_2^*} \cdot 100 \quad (4)$$

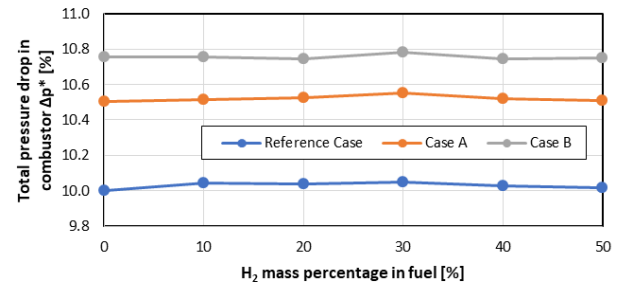


Fig. 8. Total pressure drop

Firstly, it can be noticed that regardless of the hydrogen mass fraction the pressure drop (ranging from 10.00% to 10.05%) is most advantageous in the reference case, intermediate (10.50–10.56) in case A and highest (10.74–10.78%) in case B. The total pressure drop in gas microturbine combustors of this type often amounts to about 10% [12]. The total pressure drop was expected to be higher in the IFGR cases than in the reference case as the IFGR pipe systems are extra elements, constituting additional sources of flow resistance, added to combustors A and B.

Secondly, it should be noted that the total pressure drop is quasi-constant in each case at the increasing hydrogen mass fraction in the fuel. This was also expected as the total pressure drop is closely connected with the combustor design.

Finally, the total pressure drop evolves from 10.00% (the reference case with pure methane fuel) to 10.78% (case B at a 0.3 hydrogen mass fraction in the fuel). The total pressure drop was found to increase maximally by about 0.78%. This increase in total pressure drop is very low considering the fact that the combustor internal design was modified. The differences in pressure drop between the considered IFGR cases can be neglected. Hence one can conclude that the IFGR system does not significantly affect the total pressure drop in the combustor.

Summing up, the implementation of the IFGR system into the combustor at various hydrogen fuelling options has no significant effect on the total pressure drop. This is a positive finding as keeping a low total pressure drop in the gas turbine combustor is one of the major challenges in designing. The fact that the IFGR system has no impact on this parameter is important since this means that the combustor's operating pressure will not be altered when the IFGR system is implemented.

4.3. Impact of IFGR system on temperature field

In the first part of this subsection the homogeneity of combustion static temperature is discussed. The designed combustors were considered as three-dimensional objects. In order to interpret the combustion phenomena occurring inside the combustion zone a representative plane for observing them had to be chosen. The selected plane corre-

sponded to the longitudinal cross section of the combustion chamber. The combustion static temperature field in each of the combustor design cases is shown below for pure methane fuelling (Fig. 9) and for a 0.5 hydrogen mass fraction in the methane fuel (Fig. 10).

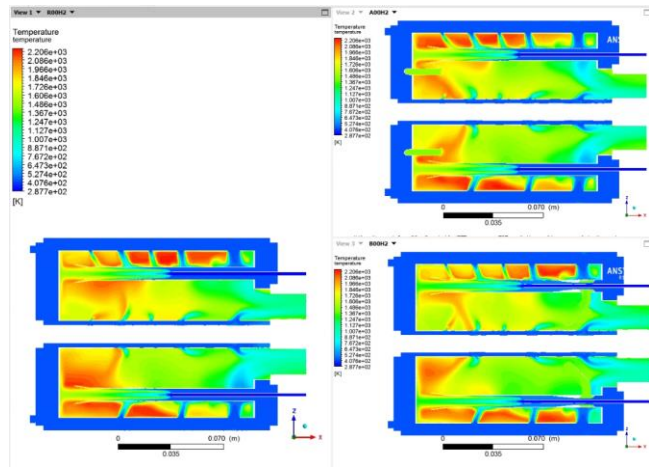


Fig. 9. Combustion static temperature field for pure methane fuelling option

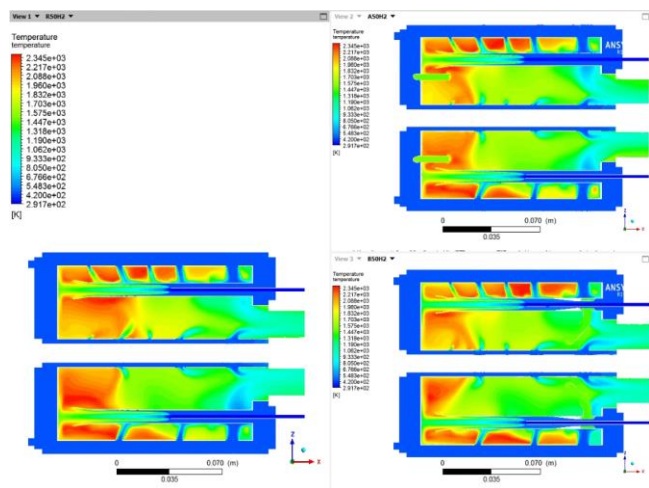


Fig. 10. Combustion static temperature field for 50% hydrogen mass percentage in fuel

Firstly, when comparing the combustion static temperature field (Figs 9 and 10) for the three cases, one can see that the hot spots are largest in the reference case, smallest in case B and intermediate in size in case A, regardless of the hydrogen mass fraction in the fuel. In all the cases the hot spots are located in the top part of the liner and along the liner’s internal walls. In case A the temperature field is situated at the central top part of the liner in the place where the exhaust gases are introduced into the combustion zone, the temperature gradient is lower and the hot-spot area is reduced in comparison with the reference case. In case B the static temperature field in the top part of the liner is more homogeneous and the hot spots are smaller than in the reference case and in case A. In case B, combustion zone homogenization in the top part of the liner occurs in the whole section, not only in the central location (as in case A). This is due to the fact that the exhaust gases are mixed

with fresh air in the mixing pipes. According to this visual analysis, case B is characterized by the best combustion static temperature field homogeneity, regardless of the hydrogen mass fraction in the fuel.

Secondly, when hydrogen is added to the fuel, the temperature gradient and the size of the hot spots increase. Thanks to the introduction of the IFGR system more homogeneous and smaller hot spots than in the reference case are obtained.

The visual observations are supported by the static temperature uniformity index on the mentioned-above plane, calculated for each of the cases at various hydrogen mass fractions. The uniformity index was calculated from formula 5.

$$UI_{\text{area}}^{\text{plane}} = 1 - \frac{\sum_{i=1}^N [(T_{\text{face}_i} - T_{\text{average}}) \cdot A_i]}{2 \cdot T_{\text{average}} \cdot \sum_{i=1}^N [A_i]} \quad (5)$$

The values of the area weighted static temperature uniformity index (UI) are presented in Fig. 11, which validates the visual analysis carried out above. Case B is characterized by the best static temperature homogeneity, while the reference case shows the worst homogeneity, regardless of the hydrogen mass fraction in the fuel. When hydrogen is added to the fuel, homogeneity degradation occurs. The uniformity index values are very similar, which indicates that the IFGR system does not significantly affect the global static temperature homogeneity on the investigated plane of the combustor.

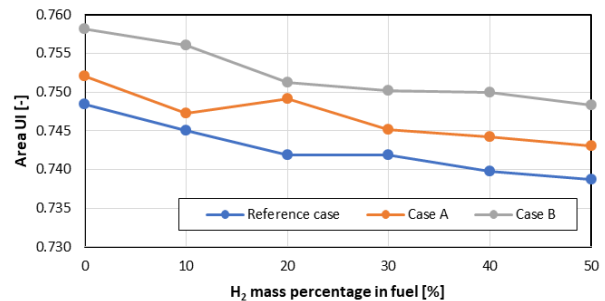


Fig. 11. Area weighted static temperature uniformity index for selected cross section

Summing up, thanks to the implementation of the IFGR system the combustion static temperature field is moderately homogenized and the size of the hot spots is reduced, especially in case B. This applies to all the hydrogen mass fractions in the fuel. The size of the hot spots and the temperature gradient increase with the amount of hydrogen added to the fuel. This applies to the selected representative cross section, but not necessarily to the whole volume of the combustor.

In the second part of this subsection, the maximum combustion static temperature is investigated. Figure 12 presents the combustion maximum static temperature occurring in the combustor.

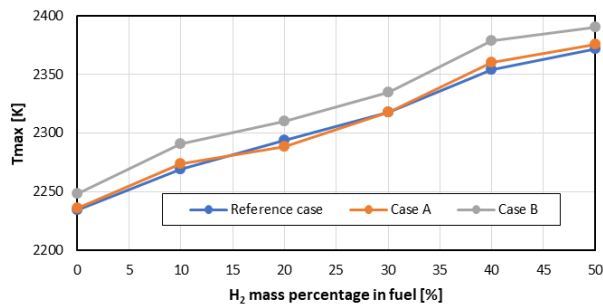


Fig. 12. Combustion maximum static temperature in combustors

Firstly, it can be noticed that the maximum combustion static temperature in the reference case and that in case A are comparable, regardless of the hydrogen mass fraction in the fuel. In case B the maximum combustion static temperature is higher than in the reference case and in case A. The similarities between the reference case and case A stem from the fact that the amount of air supplied into the combustion zone is similar in both cases (see Table 5) and the recirculated exhaust gas mass flow is lower than in case B (see Fig. 7). As the IFGR ratio is low in case A, the chemical and physical effects (described in the Introduction) of the exhaust gases on the combustion zone are very poor and additionally, not only the reference case air mass flow through the liner, but also the air-fuel equivalence ratio and the combustion volume are maintained. This contributes to the maximum combustion static temperature similarity between the reference case and case A, regardless of the hydrogen mass fraction in the fuel. In case B the maximum combustion static temperature is higher than in the reference case and in case A and also the IFGR ratios (see Fig. 7) are higher than in case A, but they are still very low (the IFGR%* ratio amounts to about 0.5%). This may indicate that the expected positive (chemical and physical) effects on the combustion processes are seriously limited. Considering that the mass flow of the recirculated exhaust gases is low, the exhaust gas enthalpy and the carbon monoxide reburn enthalpy added to the primary combustion zone can be neglected. According to the results presented in Table 5, in case B the air mass flow passing through the mixing pipes (primary combustion air) is reduced in comparison with the reference case and case A. For example, in the pure methane fuelling mode the primary air mass flow amounts to about $3.2\text{E-}2$ kg/s in the reference case, to about $3.3\text{E-}2$ kg/s in case A and to only about $1.9\text{E-}2$ kg/s in case B. The primary combustion air mass flow modification in case B was identified as a major factor contributing to a change in combustion static temperature. The modification of the air supplied into the liner can affect the air-fuel equivalence ratio repartition in graduated combustion. An increase in the maximum combustion static temperature would indicate that there is a zone inside the liner where the air-fuel equivalence ratio is close to the stoichiometric condition (case B). This hypothesis will be tested in the next section of this paper.

Secondly, it can be noticed that the maximum combustion static temperature increases as the hydrogen mass fraction in the fuel is increased. The maximum combustion static temperature evolves from 2234–2248 K to 2371–

2390 K. An increase in the maximum static temperature by about 140 K occurs when pure methane fuelling is changed to fuelling with a 0.5 hydrogen mass fraction in the fuel. The methane maximum adiabatic combustion temperature is 2250 K [14, 15], which corresponds to the result obtained in the cases with pure methane fuelling. The hydrogen maximum adiabatic combustion temperature is 2400 K [14, 15], which corresponds to the results obtained in the case with a 0.5 hydrogen mass fraction in the fuel. The increase in combustion temperature was expected for the hydrogen enriched fuel and the obtained results are consistent with the chemical and physical combustion properties of the fuel.

Summing up, one should note that the maximum combustion static temperature is lowest in the reference case and highest in case B, regardless of the hydrogen mass fraction in the fuel. At the same time the maximum combustion static temperature results for case A are closely comparable with the ones for the reference case. It emerges from the discussion of the results that the maximum combustion static temperature modification can be linked to the air-fuel equivalence ratio modification. This hypothesis will be tested in the next section of this paper. The addition of a 0.5 hydrogen mass fraction to the methane fuel provokes a rise in the maximum combustion static temperature by about 140 K. This observation is consistent with the chemical and physical combustion properties of the fuels.

In the third part of this subsection, the exhaust total temperature is analysed. This is one of the most important parameters describing a combustor. The evolution of the averaged exhaust gas total temperature is presented in Fig. 13.

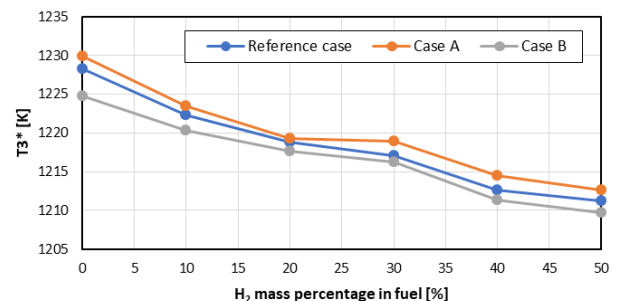


Fig. 13. Averaged exhaust gas total temperature

Firstly, it can be noticed that the averaged exhaust gas total temperature is highest in case A, lowest in case B and intermediate in the reference case, regardless of the hydrogen mass fraction in the fuel. In each of the fuelling cases the exhaust temperature values are relatively close. For example, in the pure methane fuelling mode the exhaust total temperature ranges from 1225 K to 1230 K. According to the preliminary simplified combustor calculations (see Table 1), the exhaust total temperature was to amount to about 1185 K. The relative difference in exhaust total temperature between the simplified gas microturbine design calculation result and the simulation result for the reference case amounts to about 3.65%. Considering that the design calculation model was much simplified and did not take into account the combustion chamber's shape which has a major impact on combustor exhaust total temperature, this difference is acceptable. Moreover, the difference in exhaust

total temperature between the reference case and the IFGR cases is negligible, regardless of the hydrogen mass fraction in the fuel. The fact that the exhaust total temperature remains at the same level in all the studied cases is highly important as it indicates that the implementation of the IFGR system will not alter this combustor operating parameter.

Secondly, one should note that the exhaust total temperature drops from the range of 1225–1230 K (pure methane fuelling) to the range of 1210–1213 K (for the 0.5 hydrogen mass fraction in the fuel). This means that the exhaust total temperature decreases by 15–17 K when hydrogen is added to the fuel. The decrease can be due to two factors: 1) a fuel supply calculation inaccuracy and 2) the fact that the addition of hydrogen to the fuel results in an extension of the flammability range and in incomplete combustion in the liner. This hypothesis needs to be tested since if incomplete combustion occurred in the liner, this would increase the risk of combustion in the turbine part of the gas microturbine. Although the decrease in exhaust total temperature can be neglected in terms of value, there is a need to check if this temperature drop stems from incomplete combustion. In the next subsection, for all the hydrogen mass fractions the total air-fuel equivalence ratio (in the combustion chamber) will be compared with the air-fuel equivalence ratios defining the range of flammability of the air-fuel mixture.

Summing up, one should note that the IFGR implementation does not significantly affect the exhaust total temperature, regardless of the hydrogen mass fraction in the fuel. When hydrogen is added to the methane fuel, a small decrease in exhaust total temperature occurs. Even though the decrease is negligible, it should be checked if it is linked with incomplete combustion in the liner (due to a flammability range extension caused by the addition of hydrogen to the fuel). This hypothesis will be tested in the next section of this paper.

From the above observations one can conclude that the implementation of the IFGR system into the gas microturbine combustor does not significantly affect the combustion temperature homogeneity and the exhaust total temper-

ature, but it has an impact on the maximum combustion static temperature (especially in case B). The positive effect is that the exhaust total temperature is not significantly altered when the IFGR system is implemented. The fact that the combustion static temperature homogeneity is not significantly affected by the IFGR system implementation is of neutral consequence. Finally, the conservation or even augmentation (case B) of the maximum combustion static temperature when the IFGR system is implemented is a negative effect. This effect is probably due to the modification of the air-fuel ratio, which will be checked in the next subsection of this paper.

4.4. Impact of IFGR system on lambda ratio

This section is divided in two parts. The first part is dedicated to the analysis of the air-fuel equivalence ratio, aimed at explaining the increase in the maximum combustion temperature in case B. The air-fuel equivalence ratios occurring in the combustion chamber were determined on the basis of the liner air and exhaust gas mass flow repartition and the combustion properties of the fuel (methane and hydrogen) [41–43]. The oxygen present in the exhaust gases was taken into account in the air-fuel equivalence ratio calculations. The air-fuel equivalence ratio values are presented in Table 6. The primary zone is the liner’s part which air and exhaust gases (coming from the IFGR system) enter. The hole series I to IV are perimetrical hole series located on the liner, enabling combustion to occur. The cooling hole series are holes located in the liner’s end part, letting cooling air in. The “IFGR out” designation in table 6 is the liner outlet air-fuel equivalence ratio after some of the exhaust gas is taken by the IFGR system.

According to Table 6, the air-fuel equivalence ratios are closest to unity after liner hole series no. II. Figure 14 shows the air-fuel equivalence ratios for the second liner hole series.

One should note the decrease in the amount of oxygen supplied into the primary combustion zone in IFGR combustion case B in comparison with the reference case and case A. As a result of this decrease the augmentation of the

Table 6. Air-fuel equivalence ratios

| Case | $\lambda_{\text{Prim.zone}}^{\text{Total}} [-]$ | $\lambda_{\text{Hole I}}^{\text{Total}} [-]$ | $\lambda_{\text{Hole II}}^{\text{Total}} [-]$ | $\lambda_{\text{Hole III}}^{\text{Total}} [-]$ | $\lambda_{\text{Hole IV}}^{\text{Total}} [-]$ | $\lambda_{\text{Cool.hole}}^{\text{Total}} [-]$ | $\lambda_{\text{IFGR out}}^{\text{Total}} [-]$ |
|-------|---|--|---|--|---|---|--|
| R00H2 | 0.38 | 0.53 | 1.20 | 1.35 | 2.01 | 2.96 | 2.96 |
| R10H2 | 0.39 | 0.55 | 1.24 | 1.40 | 2.10 | 3.09 | 3.09 |
| R20H2 | 0.40 | 0.56 | 1.28 | 1.44 | 2.16 | 3.18 | 3.18 |
| R30H2 | 0.40 | 0.57 | 1.30 | 1.47 | 2.21 | 3.25 | 3.25 |
| R40H2 | 0.41 | 0.58 | 1.33 | 1.50 | 2.25 | 3.32 | 3.32 |
| R50H2 | 0.42 | 0.60 | 1.36 | 1.53 | 2.29 | 3.37 | 3.37 |
| A00H2 | 0.39 | 0.54 | 1.21 | 1.36 | 2.02 | 2.97 | 2.96 |
| A10H2 | 0.40 | 0.56 | 1.25 | 1.41 | 2.10 | 3.09 | 3.09 |
| A20H2 | 0.41 | 0.57 | 1.29 | 1.45 | 2.16 | 3.18 | 3.18 |
| A30H2 | 0.42 | 0.59 | 1.32 | 1.49 | 2.22 | 3.26 | 3.25 |
| A40H2 | 0.42 | 0.60 | 1.34 | 1.52 | 2.26 | 3.33 | 3.32 |
| A50H2 | 0.44 | 0.61 | 1.37 | 1.54 | 2.30 | 3.38 | 3.37 |
| B00H2 | 0.24 | 0.40 | 1.10 | 1.27 | 1.97 | 2.97 | 2.96 |
| B10H2 | 0.25 | 0.42 | 1.15 | 1.32 | 2.05 | 3.10 | 3.09 |
| B20H2 | 0.25 | 0.43 | 1.18 | 1.36 | 2.11 | 3.19 | 3.18 |
| B30H2 | 0.26 | 0.44 | 1.21 | 1.39 | 2.16 | 3.26 | 3.25 |
| B40H2 | 0.26 | 0.45 | 1.23 | 1.42 | 2.20 | 3.33 | 3.32 |
| B50H2 | 0.27 | 0.45 | 1.26 | 1.44 | 2.24 | 3.39 | 3.37 |

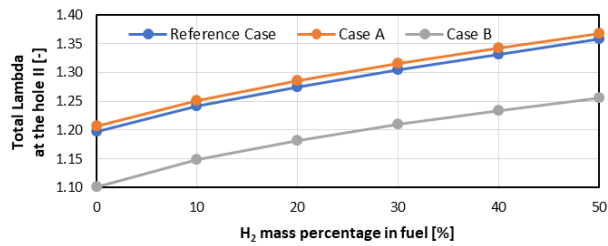


Fig. 14. Air-fuel equivalence ratios located after second liner hole series

total air-fuel equivalence ratio is delayed. Regardless of the hydrogen mass fraction in the fuel, case B has the lowest total lambda after the second liner hole series, which is closest to unity, especially in the pure methane fuelling mode. This observation is consistent with the temperature evolution described in the previous section. The augmentation of the maximum combustion static temperature in case B is connected rather with the modification of the air mass flow than with the exhaust gases recirculated by the IFGR system.

The second part of this section is dedicated to determining the evolution of the combustion zone in the studied combustor cases when hydrogen is added to the fuel. The fuel combustion ranges were determined [41–44] and compared with the air-fuel equivalence ratios in the liner's top part and its end part. As a result, it was found whether the combustion conditions were met in the two parts of the liner. The results of this analysis are presented in Table 7.

Firstly, according to the results presented in Table 7, the conditions in the primary combustion zone are met in the reference combustor and in the case A combustor when the hydrogen mass fraction in the fuel is larger than 0.2. Whereas in case B the combustion conditions in the primary combustion zone are not met. The main objective of the primary zone is to assure good air-fuel mixing in order to obtain a homogeneous mixture. Generally, combustion processes should be limited in this zone. When hydrogen, amounting to a 0.2 mass fraction, is added to the fuel, combustion occurs in the primary zone in the reference case and

in case A. Only in case B combustion does not occur in the primary zone. This is due to a primary zone air mass flow reduction connected with the venturi shaped mixing pipes (Table 5). As regards the displacement of the flame into the top zone of the liner, the IFGR system case A does not present any advantages (in comparison with the reference case) and in case B the combustion conditions are not met in the top part of the liner (but this is just due to the primary air mass flow reduction).

Secondly, the addition of hydrogen to the fuel provokes an increase in the air-fuel equivalence ratio at which combustion can occur. According to the data presented in Table 7, beginning with the first hydrogen addition (a 0.1 mass fraction) the value of the total lambda at the combustion chamber's outlet is lower than the maximum lambda value at which fuel combustion can occur. This applies to the reference case and the IFGR cases. The addition of hydrogen alters the combustion design in the liner: combustion occurs in the whole liner, even in the cooling zone. When hydrogen is added, the temperature of the exhaust gases drops (Fig. 13) because the combustion is not complete yet. There is a risk that the combustion process will continue after the mass flow leaves the combustion chamber in the turbine. This risk cannot be reduced by implementing the IFGR system since the latter does not modify the final total air-fuel equivalence ratio.

Summing up, one should note that the increase in the maximum combustion static temperature in IFGR case B stems from the air-fuel equivalence ratio modification. When hydrogen amounting to a mass fraction of over 0.2 is added to the fuel, the combustion conditions in the primary zone are met in the reference case and in IFGR case A. In IFGR case B the combustion conditions in the primary zone are not met for the whole range of hydrogen additions. The drop in exhaust total temperature after hydrogen addition is the consequence of a combustion range extension resulting in a combustion zone expansion even to the turbine's inlet.

Table 7. Primary air zone and exhaust zone lambda vs flammability limit lambda

| Case | λ_{\min} [-] | $\lambda_{\text{Prim.zone}}^{\text{Total}}$ [-] | State | $\lambda_{\text{IFGR out}}^{\text{Total}}$ [-] | λ_{\max} [-] | State |
|-------|----------------------|---|---------------|--|----------------------|---------------|
| R00H2 | 0.592 | 0.38 | No combustion | 2.96 | 1.985 | No combustion |
| R10H2 | 0.510 | 0.39 | No combustion | 3.09 | 3.441 | Combustion |
| R20H2 | 0.442 | 0.40 | No combustion | 3.18 | 4.656 | Combustion |
| R30H2 | 0.384 | 0.40 | Combustion | 3.25 | 5.685 | Combustion |
| R40H2 | 0.334 | 0.41 | Combustion | 3.32 | 6.569 | Combustion |
| R50H2 | 0.291 | 0.42 | Combustion | 3.37 | 7.335 | Combustion |
| A00H2 | 0.592 | 0.39 | No combustion | 2.96 | 1.985 | No combustion |
| A10H2 | 0.510 | 0.40 | No combustion | 3.09 | 3.441 | Combustion |
| A20H2 | 0.442 | 0.41 | No combustion | 3.18 | 4.656 | Combustion |
| A30H2 | 0.384 | 0.42 | Combustion | 3.25 | 5.685 | Combustion |
| A40H2 | 0.334 | 0.42 | Combustion | 3.32 | 6.569 | Combustion |
| A50H2 | 0.291 | 0.44 | Combustion | 3.37 | 7.335 | Combustion |
| B00H2 | 0.592 | 0.24 | No combustion | 2.96 | 1.985 | No combustion |
| B10H2 | 0.510 | 0.25 | No combustion | 3.09 | 3.441 | Combustion |
| B20H2 | 0.442 | 0.25 | No combustion | 3.18 | 4.656 | Combustion |
| B30H2 | 0.384 | 0.26 | No combustion | 3.25 | 5.685 | Combustion |
| B40H2 | 0.334 | 0.26 | No combustion | 3.32 | 6.569 | Combustion |
| B50H2 | 0.291 | 0.27 | No combustion | 3.37 | 7.335 | Combustion |

4.5. Impact of IFGR system on CO and NO_x concentrations

The CO concentrations in exhaust were calculated from formula 6 and are presented in Fig. 15.

$$CO = \frac{CO_{mole_fraction}}{1 - H_2O_{mole_fraction}} \cdot 10^6 \quad (6)$$

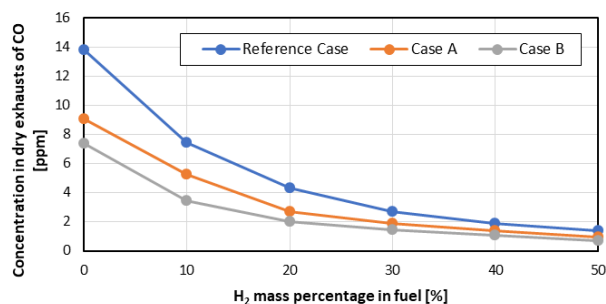


Fig. 15. CO concentrations in exhaust

Firstly, the CO concentrations show a decreasing trend from the reference case to case B. For all the IFGR cases CO concentrations are below 10 ppm. The decreasing values of CO concentrations correspond to an increase in the maximum combustion static temperature and to the recirculation of some of the exhaust gas mass flow. This reduction in CO concentrations can be due to two facts: 1) the combustion temperature increases from the reference case to case B and so the concentrations decrease and 2) some of the CO present in the exhaust gases is recirculated into the combustion zone and this CO is reburnt, which results in a reduction in CO concentration in the IFGR cases. The CO concentration trend is maintained for the whole range of hydrogen mass fractions in the fuel.

Secondly, the CO concentrations decrease as hydrogen is added to the fuel, regardless of the combustor case. This is due to the augmentation of the maximum combustion static temperature (see Fig. 12) and the degradation of combustion temperature homogeneity (see Fig. 11), resulting from hydrogen addition.

Finally, the reduction in CO concentrations is connected with the augmentation of the maximum combustion static temperature, which occurs in all the IFGR cases (especially in case B) and when hydrogen is added to the fuel.

The NO_x concentrations in exhaust were calculated from formula 7 and are presented in Fig. 16.

$$NO_x = \frac{NO_{mole_fraction} + NO_2_{mole_fraction}}{1 - H_2O_{mole_fraction}} \cdot 10^6 \quad (7)$$

Firstly, as regards NO_x concentrations, they increase from the reference case to case B. In this kind of power devices NO_x concentrations are strongly linked with the thermal NO mechanism. As the maximum combustion temperature increases from the reference case to case B (Fig. 12), so do NO_x concentrations. This is consistent with the CO concentrations and the maximum combustion temperature evolution. The NO_x concentration trend is maintained for the whole range of hydrogen mass fractions in the fuel.

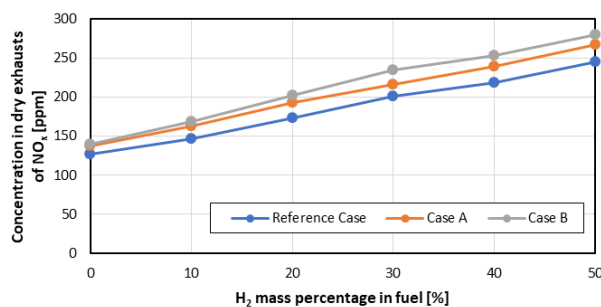


Fig. 16. NO_x concentrations in exhaust

Secondly, the NO_x concentrations decrease as hydrogen is added to the fuel, regardless of the combustor case. This is due to the augmentation of the maximum combustion static temperature (see Fig. 12) and the degradation of combustion temperature homogeneity (see Fig. 11), resulting from hydrogen addition.

Finally, the increase in NO_x concentrations in exhaust is connected with the augmentation of the maximum combustion static temperature, which occurs in all the IFGR cases (especially in case B) and when hydrogen is added to the fuel.

Summing up, the implementation of the IFGR system results in a reduction in CO concentrations and at the same time in an increase in NO_x concentrations. The most remarkable changes in pollutant concentrations in exhaust occur in case B. The changes are due to the increase in combustion temperature. The temperature augmentation is connected with the air-fuel equivalence ratio modification in the IFGR cases and with the increase in the hydrogen mass fraction in the fuel. The IFGR system does not affect the emissivity of the combustor through the expected chemical and physical effects (described in the Introduction) because the exhaust gas mass flow is too low to have a significant effect on the combustion process. The observed pollutant concentration modifications resulting from the implementation of the IFGR system are connected with the modification of the air-fuel equivalence ratio in the combustor's liner.

5. Conclusion

The observations and conclusions relating to the implementation of an autonomous IFGR system into the gas microturbine in the context of the co-combustion of higher hydrogen enriched methane fuel are listed below:

- it is possible to achieve autonomous exhaust gases recirculation inside a gas microturbine combustor at various hydrogen mass fractions in the fuel by applying an adequate IFGR pipe system;
- the maximum exhaust gases recirculation is obtained in combustor case B, regardless of the hydrogen mass fraction in the fuel;
- the IFGR ratios are constant in case A, whereas in case B they decrease as the hydrogen mass fraction in the fuel increases;
- the IFGR system design reduces the risk of overheating the IFGR pipes;
- the IFGR system implementation into the combustor does not significantly affect the total pressure drop at

- various hydrogen fuelling options – the combustor’s pressure operating parameters are not altered when the IFGR system is implemented;
- the implementation of the IFGR system into the gas microturbine combustor does not significantly affect the combustion temperature homogeneity at a constant hydrogen mass fraction in the fuel;
- the addition of hydrogen to the fuel results in the degradation of combustion static temperature homogeneity in the reference case and in the IFGR cases;
- the implementation of the IFGR system provokes maximum combustion static temperature augmentation, especially in case B, regardless of the hydrogen mass fraction in the fuel;
- the addition of hydrogen to the fuel provokes maximum combustion static temperature augmentation in all the combustor cases;
- the maximum temperature augmentation, especially in case B, is due to the fact that the local air-fuel equivalence ratio approaches unity owing to the IFGR system design;
- for a constant hydrogen mass fraction in the fuel the exhaust total temperature in the reference case and in the IFGR cases is comparable;
- the addition of hydrogen to the fuel results in a decrease in the exhaust total temperature in all the combustor cases;
- the exhaust total temperature drop after hydrogen addition is due to a combustion range extension provoking a combustion zone expansion even to the inlet of the turbine;
- when hydrogen amounting to a mass fraction of over 0.2 is added to the fuel, the combustion conditions in the mixing pipes are met in the reference case and in IFGR case A;
- in IFGR case B the combustion conditions in the mixing pipes are not met for the whole range of hydrogen additions;
- the implementation of the IFGR system results in a reduction in CO concentrations and at the same time in an increase in NO_x concentrations (especially in case B);
- the addition of hydrogen to the fuel results in a reduction in CO concentrations and at the same time in an increase in NO_x concentrations (especially in case B);
- the pollutant concentration modifications are connected with the increase in combustion temperature;
- the IFGR system does not affect the emissivity of the combustor through the expected chemical and physical effects (described in the Introduction) because the exhaust gas mass flow is too low to have a significant effect;
- the observed pollutant concentration modifications resulting from the implementation of the IFGR system are connected with the modification of the air-fuel equivalence ratio in the combustor’s liner.

The investigated IFGR system enables the recirculation of exhaust gases, but the recirculated exhaust gas mass flow is too low to act as expected on the combustion processes. The observed temperature and pollutant concentration modifications result from the modification of the combustion air-fuel equivalence ratio due to the modification of the combustor design. The autonomous IFGR system does not seem to be an efficient way of improving the combustion process in the gas microturbine combustor with or without adding hydrogen to the fuel. This concept would work if the recirculated exhaust gas mass flow was increased, for example, by an additional pumping system [12], but this would entail powering the latter and so power losses would occur. At this stage of the investigations, the MILD combustion design seems to be one of the most promising ways to reduce the combustion temperature and so the emissivity.

Nomenclature

| | | | |
|---|--|------------------------------------|---|
| A_i | area of facet defining analysed surface [m ²] | $NO_{mole_fraction}$ | nitrogen oxide mole fraction [–] |
| c | air stream velocity [m/s] | NO_x | nitrogen oxides concentrations in exhaust [ppm] |
| CO | carbon monoxide concentrations in exhaust [ppm] | $NO_{2,mole_fraction}$ | nitrogen dioxide mole fraction [–] |
| $CO_{mole_fraction}$ | carbon monoxide mole fraction [–] | p^* | total pressure [Pa] |
| c_s | fuel mass flow for pure methane fuelling mode [kg/s] | p_2^* | total pressure at combustor’s inlet [Pa] |
| $c_s^{i-H_2mass_fraction}$ | fuel mass flow for hydrogen mass fraction i in fuel [kg/s] | p_3^* | total pressure at combustor’s outlet [Pa] |
| $H_{2,mass_fraction}$ | hydrogen mass fraction in fuel [–] | Δp^* | total pressure drop in combustor [%] |
| $H_2O_{mole_fraction}$ | water vapor mole fraction [–] | UI_{area}^{plane} | area averaged uniformity index [–] |
| IFGR% | primary zone combustion IFGR ratio [%] | $T_{average}$ | average static temperature in analysed cross-section [K] |
| IFGR% * | global combustion IFGR ratio [%] | T_{face_i} | static temperature on i -th facet defining analysed surface [K] |
| LHV_{CH_4} | lower heat value of methane fuel [kJ/kg] | T_{max} | static maximum temperature in combustor [K] |
| LHV_{H_2} | lower heat value of hydrogen fuel [kJ/kg] | $T3^*$ | total exhaust temperature [K] |
| Mass percentage [%] = Mass fraction [–] × 100 | | T^* | total temperature [K] |
| \dot{m} | air mass flow entering combustor [kg/s] | $\lambda_{Hole_serie_i}^{Total}$ | total air-fuel equivalence ratio for i -th hole series location [–] |
| $\dot{m}_{fuelling_pipe}$ | air mass flow passing through fuelling pipes [kg/s] | $\lambda_{max(min)}$ | explosive limit air-fuel equivalence ratio [–] |

Bibliography

- [1] Boudellal M. Power to Gas. De Gruyter. 2018. <https://doi.org/10.1515/9783110559811>
- [2] Sterner M, Jentsch M, Holzhammer U. Energiewirtschaftliche und ökologische Bewertung eines Windgas-Angebotes. Fraunhofer Institute Report. Kassel 2011.
- [3] Fařara J-M, Modliński NJ. Internal flue gas recirculation system in the gas microturbine as a way for the co-combustion of higher enriched hydrogen fuel. In: Kudela H, Cholewiński M, Machalski A. (Eds.). II edition of the XII Conference Young Scientists In Power Engineering – Book of abstracts. 153-154. Publishing House of the Wrocław University of Science and Technology. Wrocław 2020.
- [4] Lav C, Kaul C, Singh R, Rai A. Potential of micro turbines for small scale power generation. *Int J Adv Infor Sci Tech*. 2013;2(5):35-39. <https://doi.org/10.15693/ijaist/2013.v2i5.77-81>
- [5] Jerzak W. Adiabatic flame temperature and laminar burning velocity of CH₄/H₂/air mixtures. *Archiwum Spalania*. 2011; 11(3-4):197-206. https://www.researchgate.net/publication/260244139_Adiabatic_flame_temperature_and_laminar_burning_velocity_of_CH4H2air_mixtures_in_Polish
- [6] Güthe F, García M, Burdet A. Flue gas recirculation in gas turbine: Investigation of combustion reactivity and NO_x emission. *Proceedings of the ASME Turbo Expo*. Orlando 8-12.06.2009. <https://doi.org/10.1115/GT2009-59221>
- [7] Liu F, Guo H, Smallwood G. The chemical effect of CO₂ replacement of N₂ in air on the burning velocity of CH₄ and H₂ premixed flames. *Combust Flame*. 2003;133(4):495-497. [https://doi.org/10.1016/S0010-2180\(03\)00019-1](https://doi.org/10.1016/S0010-2180(03)00019-1)
- [8] Ditaranto M, Li H, Løvås T. Concept of hydrogen fired gas turbine cycle with exhaust gas recirculation: Assessment of combustion and emissions performance. *Int J Greenh Gas Con*. 2015;(37):377-383. <https://doi.org/10.1016/j.ijggc.2015.04.004>
- [9] Engineering ToolBox. Carbon Dioxide Gas – Specific Heat. 2005. https://www.engineeringtoolbox.com/carbon-dioxide-d_974.html (accessed on 28.06.2020).
- [10] Engineering ToolBox. Water Vapor – Specific Heat. 2005. https://www.engineeringtoolbox.com/water-vapor-d_979.html (accessed on 28.06.2020).
- [11] Engineering ToolBox. Air – Specific Heat at Constant Pressure and Varying Temperature. 2004. https://www.engineeringtoolbox.com/air-specific-heat-capacity-d_705.html (accessed on 28.06.2020).
- [12] Gieras M. Miniaturowe silniki turbodozrutowe (Micro-turbojet engine). Publishing House of the Warsaw University of Technology. Warsaw 2016.
- [13] Shi B, Hu J, Peng H, Ishizuka S. Effects of internal flue gas recirculation rate on the NO_x emission in a methane/air premixed flame. *Combust Flame*. 2018;(188):199-211. <https://doi.org/10.1016/j.combustflame.2017.09.043>
- [14] Jadidi M, Moghtadernejad S, Dolatabadi A. A comprehensive review on fluid dynamics and transport of suspension/liquid droplets and particles in high-velocity oxygen-fuel (HVOF) thermal spray. *Coatings*. 2015;5(4):576-645. <https://doi.org/10.3390/coatings5040576>
- [15] Taamallah S, Vogiatzaki K, Alzahrani FM, Mokheimer EMA, Habib MA, Ghoniem AF. Fuel flexibility, stability and emissions in premixed hydrogen-rich gas turbine combustion: technology, fundamentals, and numerical simulations. *Appl Energ*. 2015;(154):1020-1047. <https://doi.org/10.1016/j.apenergy.2015.04.044>
- [16] Wang L, Qi D, Sui X, Xie X. Analysis of re influence on MILD combustion of gas turbine. *Energ Power Eng*. 2013;(5):92-96. <https://doi.org/10.4236/epe.2013.54B018>
- [17] Karpiński B, Szkodo M, Staścik J et al. High temperature air combustion. *Energetyka*. 2014;12(726):735-737.
- [18] Mi J, Li P, Wang, F., Cheong K-P, Wang G. Review on MILD combustion of gaseous fuel: its definition, ignition, evolution, and emissions. *Energ Fuel*. 2021;35(9):7572-7607. <https://doi.org/10.1021/acs.energyfuels.1c00511>
- [19] Mameri A, Tabet F, Aggab Y et al. MILD Combustion of hydrogenated biogas in opposed jet configuration. *Proceedings of the 2nd International Workshop on CFD and Biomass Thermochemical Conversion*. Leipzig 9.09.2016. https://www.researchgate.net/publication/340310099_MILD_Combustion_of_hydrogenated_biogas_in_opposed_jet_configuration
- [20] Webera W, Guptab AK, Mochidac S. High temperature air combustion (HiTAC): how it all started for applications in industrial furnaces and future prospects. *Appl Energ*. 2020;(278):115551. <https://doi.org/10.1016/j.apenergy.2020.115551>
- [21] Fortunato V, Giraldo A, Rouabah M, Nacereddine R, Delanaye M, Parente A. Experimental and numerical investigation of a MILD combustion chamber for micro gas turbine applications. *Energies*. 2018;11(12):3363. <https://doi.org/10.3390/en11123363>
- [22] Albin T, Aguiar Da Franca A, Varea E et al. Potential and challenges of MILD combustion control for gas turbine applications. In: King R. (Eds.). *Active Flow and Combustion Control – Notes on Numerical Fluid Mechanics and Multi-disciplinary Design*. 2015, 127. Springer.
- [23] Ansys website. <https://www.ansys.com/> (accessed on 25.05.2021).
- [24] Gieras M, Stańkowski T. Computational study of an aerodynamic flow through a micro turbine engine combustor. *J Power Technol*. 2012;92(2):68-79.
- [25] Suchocki T, Lampart P, Klonowicz P. Numerical investigation of a GTM 140 turbojet engine. *Open Eng*. 2015;(5): 478-484. <https://doi.org/10.1515/eng-2015-0053>
- [26] Dias FLG, Do Nascimento MAR, De Oliveira Rodrigues L. Reference area investigation in a gas turbine combustion chamber using CFD. *J Mech Eng Autom*. 2014;4(2):73-82. <https://doi.org/10.5923/j.jmea.20140402.04>
- [27] Vilag V, Vilag J, Carlanescu R, Mangra A, Florean F. CFD application for gas turbine combustion simulations. In: Ji G., Zhu J. (Eds.). *Computational Fluid Dynamics Simulations*. IntechOpen. 2019. <https://doi.org/10.5772/intechopen.89759>
- [28] Gonzalez C, Wong KC, Armfield S. Computational study of a micro turbine engine combustor using Large Eddy Simulation and Reynolds Averaged turbulence models. *ANZIAM Journal*. 2008;49(2007):407-422. <https://doi.org/10.21914/anziamj.v49i0.338>
- [29] Sosnowski M, Krzywanski J, Gnatowska R. Polyhedral meshing as an innovative approach to computational domain discretization of a cyclone in a fluidized bed CLC unit. *E3S Web Conf*. 2017;(14):01027. <https://doi.org/10.1051/e3sconf/20171401027>
- [30] Qureshi Z, Chan A. A study of the effect of element types on flow and turbulence characteristics around an isolated high-rise building. *Eleventh International Conference on CFD in the Minerals and Process Industries*. CSIRO. Melbourne 7-9.12.2015. https://www.cfd.com.au/cfd_conf15/PDFs/035IQB.pdf

- [31] Matyushenko A, Stabnikov A, Garbaruk A. Criteria of computational grid generation for turbulence models taking into account laminar-turbulent transition. *J Phys: Conf Ser.* 2019;(1400):077047. <https://doi.org/10.1088/1742-6596/1400/7/077047>
- [32] Ansys, Inc. *Ansys Fluent Theory Guide – Release 15.0.* 2013.
- [33] Suchocki T, Lampart P, Surwilo J. Designation of operating characteristics for micro-jet engine and CFD validation. *Mechanik.* 2015;(7):813-820. <https://doi.org/10.17814/mechanik.2015.7.301>
- [34] Smith T, Shen Z, Friedman J. Evaluation of coefficients for the weighted sum of gray gases model. *J Heat Transfer.* 1982;104(4):602-608. <https://doi.org/10.1115/1.3245174>
- [35] Fuchs F, Meidinger V, Neuburger N, Reiter T, Zündel M, Hupfer A. Challenges in designing very small jet engines fuel distribution and atomization. *International Symposium on Transport Phenomena and Dynamics of Rotating Machinery.* Honolulu 10-15.04.2016. <https://hal.archives-ouvertes.fr/hal-01891309/document>
- [36] Peters N. *Turbulent Combustion.* Cambridge University Press. 2000.
- [37] Smith GP, Golden DM, Frenklach M et al. Welcome to the GRI-Mech Home Page! http://www.me.berkeley.edu/gri_mech/ (accessed on 25.05.2021).
- [38] Ji C, Du W, Yang J, Wang S. A comprehensive study of light hydrocarbon mechanisms performance in predicting methane/hydrogen/air laminar burning velocities. *Int J Hydrogen Energ.* 2017;(42):17260-17274. <https://doi.org/10.1016/j.ijhydene.2017.05.203>
- [39] Launder BE, Spalding DB. The numerical computation of turbulent flows. *Comput Method Appl M.* 1974;3(2):269-289. [https://doi.org/10.1016/0045-7825\(74\)90029-2](https://doi.org/10.1016/0045-7825(74)90029-2)
- [40] Ansys, Inc. *Ansys Fluent Tutorial Guide – Release 18.0.* Ansys 2017.
- [41] Air liquid. *Gas encyclopedia – Méthane.* 2021. <https://encyclopedia.airliquide.com/fr/methane> (accessed on 19.06.2021).
- [42] Air liquid. *Gas encyclopedia – Hydrogène.* 2021. <https://encyclopedia.airliquide.com/fr/hydrogene> (accessed on 19.06.2021).
- [43] Air liquid. *Gas encyclopedia – Oxygène.* 2021. <https://encyclopedia.airliquide.com/fr/oxygene> (accessed on 19.06.2021).
- [44] PDF4PRO. AFC International, Inc. – *Gas Detection&Air Monitoring Specialists – Combustibles.* 2017. <https://pdf4pro.com/view/combustible-gas-chart-596617.html> (accessed on 20.06.2021).

Jean-Marc Fafara, MEng. – Faculty of Mechanical and Power Engineering, Wrocław University of Science and Technology.

e-mail: jean-marc.fafara@pwr.edu.pl



Norbert Modliński, DSc., DEng. – Faculty of Mechanical and Power Engineering, Wrocław University of Science and Technology.

e-mail: norbert.modlinski@pwr.edu.pl

